Available online at www.sciencedirect.com

SciVerse ScienceDirect

Acta Materialia 60 (2012) 1395–1407

Acta MATERIALIA

www.elsevier.com/locate/actamat

Stress-driven migration of simple low-angle mixed grain boundaries

A.T. Lim [a], M. Haataja [a,*], W. Cai [b], D.J. Srolovitz [c]

[a] Department of Mechanical and Aerospace Engineering, Princeton University, Princeton, NJ 08544, USA
[b] Mechanical Engineering Department, Stanford University, Stanford, CA 94305, USA
[c] Institute for High Performance Computing, 1 Fusionopolis Way, Singapore 138632, Singapore

Received 12 October 2011; received in revised form 15 November 2011; accepted 17 November 2011
Available online 22 December 2011

Abstract

We investigated the stress-induced migration of a class of simple low-angle mixed grain boundaries (LAMGBs) using a combination of discrete dislocation dynamics simulations and analytical arguments. The migration of LAMGBs under an externally applied stress can occur by dislocation glide, and was observed to be coupled to the motion parallel to the boundary plane, i.e. tangential motion. Both the migration and tangential velocities of the boundary are directly proportional to applied stress but independent of boundary misorientation. Depending on the dislocation structure of the boundary, either the migration or tangential velocity of the boundary can switch direction at sufficiently high dislocation climb mobility due to the dynamics of dislocation segments that can climb out of their respective slip planes. Finally, we show that the mobility of the LAMGBs studied in this work depends on the constituent dislocation structure and dislocation climb mobility, and is inversely proportional to misorientation.

Keywords: Grain boundary migration; Dislocation dynamics simulation; Dislocation boundaries

1. Introduction

Grain boundary migration is one of the most fundamental phenomena underlying microstructural evolution processes, such as grain growth, recrystallization and plastic deformation of polycrystalline materials. Because of the complexity of grain boundary structure, it has not been possible to develop a predictive model for the mobility of grain boundaries having arbitrary bicrystallography. Although considerable advances have been achieved in theoretical modeling and experimental characterization of the properties and behavior of very simple low-angle grain boundaries, high-angle grain boundaries with special orientations, and twin boundaries [1], the structure and mechanism of migration for a general grain boundary is not well understood.

However, if the misorientation between adjoining grains is small, the grain boundary structure is relatively simple; in particular, a low-angle grain boundary (LAGB) can be described as an array of lattice dislocations [2]. The migration of such boundaries should be describable in terms of the collective motion of its constituent dislocations. This approach has previously been employed to investigate the migration of low-angle tilt boundaries, for which parallel edge dislocations that constitute the boundaries are represented as points moving in the plane perpendicular to the dislocation lines (i.e. in two dimensions) [3].

In this paper, we provide a systematic analysis of a much more general set of grain boundaries, namely mixed tilt/twist grain boundaries consisting of curved, intersecting dislocations with multiple Burgers vectors in the experimentally relevant three-dimensional case. In particular, we focus on the stress-driven migration of a series of (1 0 0)[1 1 0] and (1 1 1)[1 1 0] mixed boundaries, initially consisting of dislocations with the smallest lattice Burgers vector in body-centered cubic (bcc) crystals.

Although almost 60 years have elapsed since the stress-induced migration of a low-angle tilt boundary was first observed experimentally by Washburn and Parker [4],

* Corresponding author.
E-mail address: mhaataja@princeton.edu (M. Haataja).

1359-6454/$36.00 © 2011 Acta Materialia Inc. Published by Elsevier Ltd. All rights reserved.
doi:10.1016/j.actamat.2011.11.032

systematic studies of the mobility of low-angle mixed grain boundaries (LAMGBs) are rather limited in both scope and number. Except for a very recent experimental investigation of stress-induced migration of a mixed boundary by Gorkaya et al. [5] and molecular dynamics simulations of a small number of mixed boundaries [6,7], all other theoretical and experimental studies of boundary mobility are for either pure tilt boundaries [8–22], pure twist boundaries [23,24], or a finite selection of tilt and twist coincidence site lattice boundaries [25]. While an arbitrary LAGB can simultaneously have both tilt and twist character, the difficulty in preparing bicrystals with LAMGBs having well-characterized dislocation structures is one reason for the lack of experimental measurements of mobility for this most common class of LAGBs.

This difficulty in preparing such bicrystals does not extend to theoretical investigations. Indeed, grain boundaries can unambiguously be represented by arrays of lattice dislocations that can relax into equilibrium LAGB structures. Describing LAGBs in this manner enables the use of discrete dislocation dynamics simulation methods to investigate the migration of such boundaries. This is the approach employed in the present study to determine the structure, migration mechanism and mobility of LAMGBs (which necessarily consist of non-parallel dislocations that may react to form dislocation segments of new Burgers vectors).

In the present work, we drive the migration of nominally planar LAMGBs via an externally applied stress to investigate how the dynamics of the constituent dislocation structure (i.e. the LAGB structure) controls boundary migration over a wide range of applied stress and dislocation climb mobility (temperature) for several misorientations using three-dimensional dislocation dynamics simulation methods. The main objective of this study is to establish the relationship between the mobility of an LAMGB and its constituent dislocation structure, and to develop a predictive model for the intrinsic mobility of such LAGBs. Such quantitative theoretical predictions are only possible for LAGBs (and possibly a small number of high-symmetry, higher-angle boundaries) because of the relative simplicity of such grain boundary structures.

The simulations and theoretical analysis presented herein demonstrate that simple LAMGBs migrate under an externally applied shear stress by means of the glide, climb, and rearrangement of the constituent dislocations. A common feature to all simple LAMGBs studied in this work is that the boundary mobilities are not dislocation-climb limited. In addition, we observe that all LAMGBs in the present study translate with components perpendicular (i.e. migration) and parallel to the boundary plane. At a fixed temperature and stress, the velocity of the boundary is independent of the misorientation, although the driving force on the boundary increases linearly with misorientation; thus, the intrinsic mobility tensor for such an LAMGB is inversely proportional to the misorientation. Intriguingly, the magnitude of boundary motion depends on the temperature at fixed applied stress, and may even switch direction as a function of temperature.

The remainder of this paper is organized as follows. In Section 2, we present our simulation method and describe how the LAMGBs are constructed. Section 3 contains the main simulation results: the relaxed structures of the LAMGBs, the dislocation structures of the moving boundaries, as well as the parallel and perpendicular components of the grain boundary velocity as a function of dislocation climb mobility (temperature), applied stress, and misorientation for both (1 0 0)[1 1 0] and (1 1 1)[1 1 0] mixed boundaries. These results are then analyzed and interpreted within a theoretical framework developed in Section 4. Finally, the implications of the simulation results and theoretical analyses to the stress-driven migration behavior of a broader class of LAMGBs are discussed in Section 5.

2. Simulation method

To simulate the migration of a LAMGB, we employed a three-dimensional dislocation dynamics technique that accounts for dislocation topology changes arising from general forces and reactions between dislocation segments as implemented within the Parallel Dislocation Simulator (ParaDiS) code [26,27]. ParaDiS is initialized by providing a dislocation network that is discretized into a series of linear segments that meet at nodes. The dynamics of the dislocation network are then simulated within the framework of isotropic linear elasticity, by calculating the force on each node arising from external and internal forces on adjacent linear segments, and subsequently evolving the position of the nodes using a nodal equation of motion. In this work, we assume that the velocity of each segment is directly proportional to the driving force. In the course of the simulation, topological changes are accommodated via addition and removal of nodes: new nodes are added and existing nodes are removed when (1) nodes on a dislocation line segment become too far apart or too close together and (2) during a reaction event when dislocation line segments merge, split or annihilate one another.

The Peach–Kohler force (per unit length) [28] is determined from the total stress $\boldsymbol{\sigma}_i$ on the ith linear segment having Burgers vector $\mathbf{b}_i$ and line direction $\hat{\boldsymbol{\xi}}_i$ as:

$$\mathbf{f}_i = (\boldsymbol{\sigma}_i \cdot \mathbf{b}_i) \times \hat{\boldsymbol{\xi}}_i. \tag{1}$$

Assuming overdamped dislocation motion, the velocity of the ith segment may be written as:

$$\mathbf{v}_i = \mathbf{M}_i \cdot \mathbf{f}_i, \tag{2}$$

where $\mathbf{M}_i$ denotes a mobility tensor that accounts for the glide mobility of screw dislocations (m_s), the glide mobility of edge dislocations (m_g) and the climb mobility of edge dislocations (m_c). In this study, we set the glide mobility of screw and edge dislocations to be equal, i.e. $m_s = m_g$

(this is reasonable for bcc metals at high temperatures), and construct the mobility tensor to interpolate smoothly between glide and climb motion (see Ref. [29] for details):

$$\mathbf{M}_i = m_g(\mathbf{I} - \hat{\mathbf{n}}_i \otimes \hat{\mathbf{n}}_i) + M_c \hat{\mathbf{n}}_i \otimes \hat{\mathbf{n}}_i, \quad (3)$$

where $\mathbf{I}$ is the identity matrix, $\hat{\mathbf{n}}_i = (\mathbf{b}_i \times \hat{\boldsymbol{\xi}}_i)/|\mathbf{b}_i \times \hat{\boldsymbol{\xi}}_i|$ denotes the slip plane normal of the ith linear segment, $M_c = [m_g^{-2} + (m_c^{-2} - m_g^{-2})\sin^2\alpha_i]^{-1/2}$, and $\alpha_i = \mathbf{b}_i \angle \hat{\boldsymbol{\xi}}_i$ denotes the angle between vectors $\mathbf{b}_i$ and $\hat{\boldsymbol{\xi}}_i$.

In the ParaDiS implementation of discrete dislocation dynamics, the position, orientation and length of each dislocation line segment evolves with time as the nodes terminating the segment at each end advance according to their respective equation of motion. To find the position of every node at each time step, the nodal equation of motion is integrated numerically using the Euler-trapezoid method.

LAMGBs were constructed in accordance with Frank's fomula [2] using bcc lattice dislocations. Although the boundaries are free of long-range stresses (as mandated by Frank's formula), the dislocation configuration of each boundary was allowed to fully relax within an isotropic solid with shear modulus μ and Poisson ratio $\nu = 1/3$ (the dislocations move as a result of reactions and internal stresses between dislocation segments) prior to being subjected to a constant external stress τ that drives the boundary to migrate. To investigate the correlation between the dislocation structure of the boundary and its mobility, we evaluate the boundary velocity $\mathbf{V}$ as a function of applied stresses in the $0 < \tau \leqslant 0.05\,\mu$ range, dislocation climb mobility $0 \leqslant m_c \leqslant m_g$, and misorientation angle $\theta = \{2.0°, 4.0°\}$. The details of the dislocation structure and corresponding boundary parameters for the LAMGBs considered here are given in Appendix A.

In this paper, we focus on simple LAMGBs, for which the magnitude of the lattice Burgers vectors and dislocation spacing in each set are equal, i.e. $b_1 = b_2 = b$ and $D_1 = D_2 = D$. In particular, $\mathbf{b}_1$ and $\mathbf{b}_2$ are chosen from the set of $\frac{a}{2}\langle 1\,1\,1\rangle$ Burgers vectors, typical of bcc metals. It is important to note that with such specialized Burgers vectors and dislocation line spacings, it follows (see Appendix A) that the orientation of the boundary plane is no longer arbitrary but, in fact, is constrained by:

$$\hat{\boldsymbol{\nu}} \cdot (\mathbf{b}_1 \pm \mathbf{b}_2) = 0. \quad (4)$$

The restrictions (i.e. $b_1 = b_2 = b$ and $D_1 = D_2 = D$) on the LAMGB dislocation structure imply that the boundary normal $\hat{\boldsymbol{\nu}}$ must be perpendicular to either $\mathbf{b}_1 + \mathbf{b}_2$, or $\mathbf{b}_1 - \mathbf{b}_2$. In this work, we will focus on these two classes of simple LAMGBs. Although these boundaries make up a subset within the broader category of general mixed LAMGBs, their dislocation networks are complex enough to impart intriguing features to the intrinsic boundary mobility, and yet amenable to a thorough analysis. By construction, a simple LAMGB initially corresponds to a lozenge network of $\left(\mathbf{b}_1, \hat{\boldsymbol{\xi}}_1\right)$ and $\left(\mathbf{b}_2, \hat{\boldsymbol{\xi}}_2\right)$ dislocation arrays. However, this dislocation configuration is not energetically stable, as $\mathbf{b}_1$ and $\mathbf{b}_2$ segments will react to form a third segment $\mathbf{b}_3 = \mathbf{b}_1 + \mathbf{b}_2 \in a\langle 1\,0\,0\rangle$. This reaction is energetically favorable because $b_3^2 < b_1^2 + b_2^2$, and it transforms the lozenge network into a hexagonal network also seen in experiments [30].

Regardless of the dislocation structure, the boundary is constructed so that it lies in the yz-plane in the simulation box, i.e. $\hat{\mathbf{x}} = \hat{\boldsymbol{\nu}}$, with the line directions symmetric about the z-axis (see Appendix B). For each set of boundaries considered here, there is only one component of the externally applied stress $\boldsymbol{\sigma}^0$ that gives a net driving force for migration $F_\perp$, i.e. $\sigma^0_{xk} = \sigma^0_{kx}$ with $k \neq x$ (see Appendix C). For the boundary plane determined by $\hat{\boldsymbol{\nu}} \cdot (\mathbf{b}_1 + \mathbf{b}_2) = 0$, the boundary migrates under the stress component σ^0_{xz}. On the other hand, for the boundary plane determined by $\hat{\boldsymbol{\nu}} \cdot (\mathbf{b}_1 - \mathbf{b}_2) = 0$, the boundary migrates under the stress component σ^0_{xy}.

In the present simulations, we examine the stress-induced migration of two series of simple LAMGBs in a bcc crystal, one for each case in Eq. (4). Both boundaries are modeled using two sets of $\frac{a}{2}\langle 1\,1\,1\rangle$ dislocations in the $\{1\,1\,0\}$ slip planes for each boundary.

We first consider the $\hat{\boldsymbol{\nu}} \cdot (\mathbf{b}_1 + \mathbf{b}_2) = 0$ case, for which the Burgers vector and line direction pairs are $\mathbf{b}_1 = \frac{a}{2}[\bar{1}\,1\,1]$, $\hat{\boldsymbol{\xi}}_1 = \frac{1}{\sqrt{2}}[0\,1\,1]$ and $\mathbf{b}_2 = \frac{a}{2}[1\,\bar{1}\,1]$, $\hat{\boldsymbol{\xi}}_2 = \frac{1}{\sqrt{2}}[0\,\bar{1}\,1]$. The corresponding boundary plane is $(1\,0\,0)$, for which Frank's formula (Eqs. (A.3) and (A.4)) yields a rotation axis $\hat{\mathbf{u}} = \frac{1}{\sqrt{2}}[1\,1\,0]$ about which the grains adjacent to this boundary are misorientated by $\theta = a\ D^{-1}$. This is the $(1\,0\,0)[1\,1\,0]$ mixed boundary case. The twist angle of this boundary is 45°, which corresponds to 50% twist character. The periodicity of the system along the $\hat{\mathbf{y}}$ and $\hat{\mathbf{z}}$ is $L_y = L_z = L$. For this boundary to migrate, stress must be applied along the $[1\,0\,0]$ direction in the $(0\,0\,1)$ plane (i.e. $\sigma^0_{xz} = \sigma^0_{zx}$).

Next, we consider the $\hat{\boldsymbol{\nu}} \cdot (\mathbf{b}_1 - \mathbf{b}_2) = 0$ case, for which the Burgers vectors and line directions are $\mathbf{b}_1 = \frac{a}{2}[\bar{1}\,1\,1]$, $\hat{\boldsymbol{\xi}}_1 = \frac{1}{\sqrt{2}}[\bar{1}\,0\,1]$ and $\mathbf{b}_2 = \frac{a}{2}[1\,\bar{1}\,1]$, $\hat{\boldsymbol{\xi}}_2 = \frac{1}{\sqrt{2}}[0\,\bar{1}\,1]$. Except for $\hat{\boldsymbol{\xi}}_1$, the Burgers vectors $\mathbf{b}_1$ and $\mathbf{b}_2$, and line direction $\hat{\boldsymbol{\xi}}_2$ are the same as that for the $(1\,0\,0)[1\,1\,0]$ mixed boundary. Accordingly, the rotation axis is $\hat{\mathbf{u}} = \frac{1}{\sqrt{2}}[1\,1\,0]$, while the boundary plane and misorientation are $(1\,1\,1)$ and $\theta = \sqrt{3}a(2D)^{-1}$, respectively. This is the $(1\,1\,1)[1\,1\,0]$ mixed boundary case. The twist angle of this boundary is 54.7°, which corresponds to 66.7% twist character. The periodicity of the system along the $\hat{\mathbf{y}}$ and $\hat{\mathbf{z}}$ is $L_z = \sqrt{3}L_y$. For this boundary to migrate, stress must be applied along the $[1\,1\,1]$ direction in the $(\bar{1}\,1\,0)$ plane (i.e. $\sigma^0_{xy} = \sigma^0_{yx}$).

3. Results

3.1. Relaxation

When the initial (lozenge) network for each configuration is allowed to relax, the simulations show that $\mathbf{b}_1$ and $\mathbf{b}_2$ react at the intersections, producing new segments with Burgers vector $\mathbf{b}_3 = \mathbf{b}_1 + \mathbf{b}_2$ and line direction $\hat{\boldsymbol{\xi}}_{r3}$ that is parallel to $\hat{\mathbf{z}}$. The reaction proceeds until the line tension

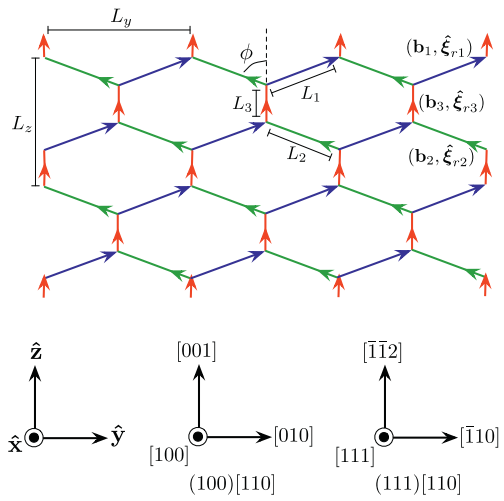

Fig. 1. Schematic representation of the equilibrium LAMGB constructed using two intersecting $\frac{a}{2}\langle 1\,1\,1\rangle$ dislocations, i.e. $\mathbf{b}_1 = \frac{a}{2}[\bar{1}\,1\,1]$ and $\mathbf{b}_2 = \frac{a}{2}[1\,\bar{1}\,1]$, which react to form a new $a[0\,0\,1]$ segment for $\mathbf{b}_3$, and the coordinate directions of the simulation box for the (1 0 0)[1 1 0] and (1 1 1)[1 1 0] mixed boundary.

forces at the triple junctions as well as the interaction forces between segments balance. A schematic illustration of the relaxed dislocation structure for both (1 0 0)[1 1 0] and (1 1 1)[1 1 0] mixed boundaries is shown in Fig. 1.

While the projection of the dislocation configuration on the mean boundary plane is a hexagonal network (see Figs. 2a and 3a), close examination of each boundary in Figs. 2b and 3b shows that the $\mathbf{b}_1$ and $\mathbf{b}_2$ segments do not remain perfectly straight. Instead, these dislocation segments weave in and out of the mean boundary plane in order to increase the net screw character and reduce the total energy of the configuration. As a result, the boundary acquires a finite width that scales in proportion to the periodicity of the dislocation structure (and hence inversely proportional to the boundary misorientation). Nevertheless, for the range of misorientations under consideration here, the width of each boundary is less than the dislocation core radius. Therefore, the mixed boundaries studied here can be considered to be macroscopically flat hexagonal networks, characterized by the angle between $\mathbf{b}_1$ and $\mathbf{b}_2$ segments, i.e. $\hat{\boldsymbol{\xi}}_{r1}\angle\hat{\boldsymbol{\xi}}_{r2} = 2\phi$, at the dislocation triple junctions. Nonetheless, for very low misorientations, such non-planarity may be significant.

Upon relaxation of the (1 0 0)[1 1 0] boundary, the resulting $\mathbf{b}_3$ segment is a pure screw dislocation. The angle between the $\mathbf{b}_1$ and $\mathbf{b}_2$ segments is $\hat{\boldsymbol{\xi}}_{r1}\angle\hat{\boldsymbol{\xi}}_{r2} = 106.2^\circ$. On the other hand, for the (1 1 1)[1 1 0] boundary, $\left(\mathbf{b}_3, \hat{\boldsymbol{\xi}}_{r3}\right)$ is a mixed segment having Burgers vector $\mathbf{b}_3 = [0\,0\,1]$ and line direction $\hat{\boldsymbol{\xi}}_{r3} = \frac{1}{\sqrt{6}}[\bar{1}\,\bar{1}\,2]$, with $\hat{\boldsymbol{\xi}}_{r1}\angle\hat{\boldsymbol{\xi}}_{r2} = 97.77^\circ$.

3.2. Migration

Simulations were performed in which both boundaries were subjected to each of the six independent components of a symmetric stress tensor (simulation frame). The simulations confirm that these simple LAMGBs can migrate only if the external shear stress is $\tau = \sigma^0_{xz}$ for $\hat{\boldsymbol{\nu}} \cdot (\mathbf{b}_1 + \mathbf{b}_2) = 0$ and $\tau = \sigma^0_{xy}$ for $\hat{\boldsymbol{\nu}} \cdot (\mathbf{b}_1 - \mathbf{b}_2) = 0$. Under such shear stress, each boundary achieves a steady-state velocity $\mathbf{V}$ (measured by averaging the velocities of the dislocation triple junction nodes). For both boundaries, the steady-state migration of the boundary perpendicular to the mean boundary plane $\mathbf{V}_\perp = V_\perp\hat{\mathbf{x}}$ is coupled to a steady-state translation of the grain boundary dislocation network in a direction that is tangential to the mean boundary plane $\mathbf{V}_\parallel$, i.e. $\mathbf{V} = \mathbf{V}_\perp + \mathbf{V}_\parallel$. The directions of the tangential velocity vectors are different for the two boundaries.

For the (1 0 0)[1 1 0] boundary, the tangential velocity is perpendicular to the $\left(\mathbf{b}_3, \hat{\boldsymbol{\xi}}_{r3}\right)$ (screw) segment, i.e. $\mathbf{V}_\parallel = V_\parallel\hat{\mathbf{y}}$. The perpendicular (migration) and tangential velocities are shown in Figs. 4 and 5, respectively, as a function of the applied stress $\tau = \sigma^0_{xz}$ for several values of dislocation climb mobility m_c and grain boundary misorientation θ. We observe that this boundary can migrate by dislocation glide,

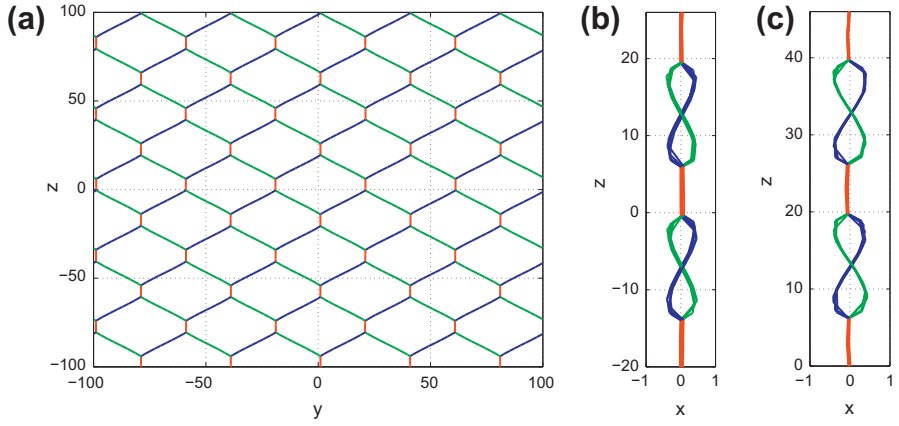

Fig. 2. Projected views (in units of lattice constant a) of dislocation configuration for the (1 0 0)[1 1 0] LAMGB at $\theta = 2.0^\circ$ misorientation onto (a) the yz-plane in the absence of applied stress as well as during migration, (b) the xz-plane in the absence of applied stress, and (c) the xz-plane during migration. The dislocation configuration during migration is very similar to that in the absence of an applied stress. In both cases, the width of the boundary is comparable to the length of the Burgers vector.

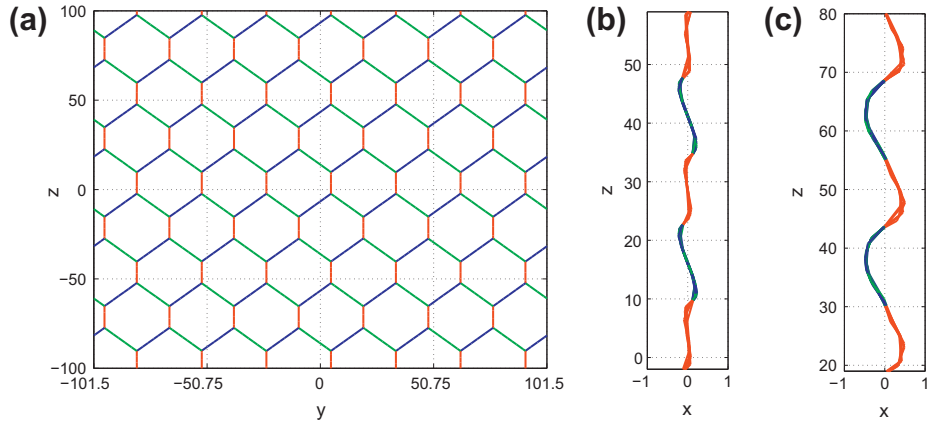

Fig. 3. Projected views (in units of lattice constant a) of dislocation configuration for the (1 1 1)[1 1 0] LAMGB at $\theta = 2.0°$ misorientation onto (a) the yz -plane in the absence of applied stress as well as during migration, (b) the xz -plane in the absence of applied stress, and (c) the xz -plane during migration. The dislocation configuration during migration is very similar to that in the absence of an applied stress. In both cases, the width of the boundary is comparable to the length of the Burgers vector.

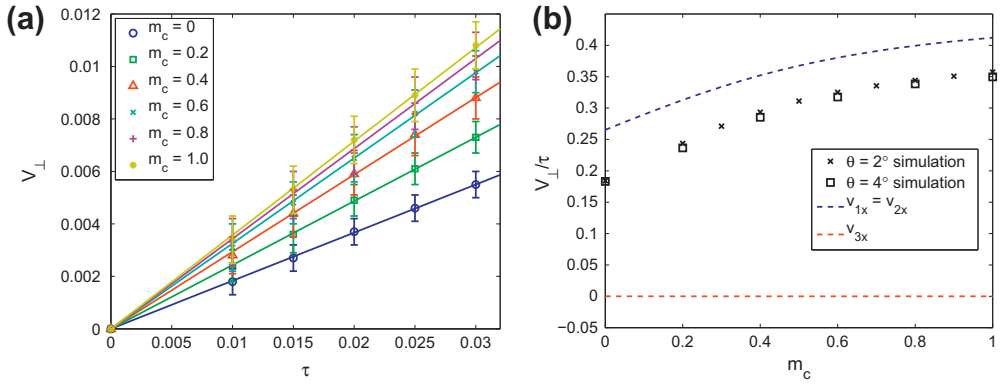

Fig. 4. (a) Steady-state (1 0 0)[1 1 0] LAMGB migration (perpendicular to the boundary) velocity $V_\perp$ (in units of $a\mu m_g$) as a function of the applied stress τ (in units of μ) for several values of dislocation climb mobility m_c (in units of m_g) at misorientation $\theta = 2.0°$. (The error bars indicate the range of velocity due to numerical fluctuations in the simulation box.) (b) The ratio of $V_\perp$ to τ as a function of m_c for $\theta = 2.0°$ and $\theta = 4.0°$. Here, v_{1x}, v_{2x} and v_{3x} denote the dislocation segment velocities along the direction perpendicular to the boundary that would result from the external force alone (see Section 4.2).

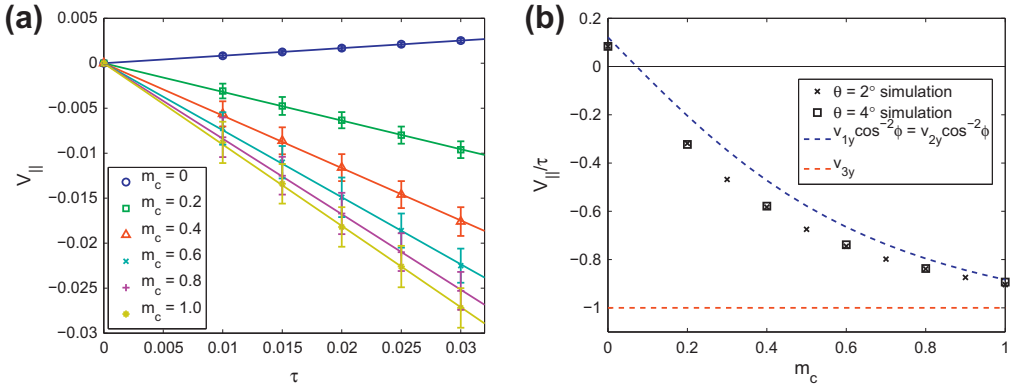

Fig. 5. (a) Steady-state (1 0 0)[1 1 0] LAMGB tangential velocity $V_\parallel$ (in units of $a\mu m_g$) (in the direction perpendicular to the $\mathbf{b}_3$ screw segment and along the boundary plane) as a function of the applied stress τ (in units of μ) for several values of dislocation climb mobility m_c (in units of m_g) at misorientation $\theta = 2.0°$. (b) The ratio of $V_\parallel$ to τ as a function of m_c for $\theta = 2.0°$ and $\theta = 4.0°$. Here, $v_{1y}\cos^{-2}\phi$, $v_{2y}\cos^{-2}\phi$, and v_{3y} denote the dislocation segment velocities along the boundary plane that would result from the external force alone, corrected by the geometrical factor $\cos^2\phi$ (see Section 4.2).

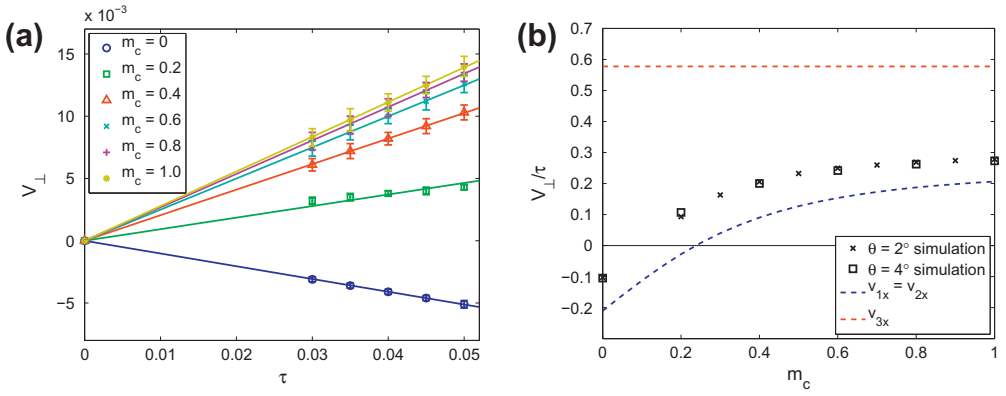

Fig. 6. (a) Steady-state (1 1 1)[1 1 0] LAMGB migration (perpendicular to the boundary) velocity $V_\perp$ (in units of $a\,\mu m_g$) as a function of the applied stress τ (in units of μ) for several values of dislocation climb mobility m_c (in units of m_g) at misorientation $\theta = 2.0°$. (The error bars indicate the range of velocity due to numerical fluctuations in the simulation box.) (b) The ratio of $V_\perp$ to τ as a function of m_c for $\theta = 2.0°$ and $\theta = 4.0°$. Again, v_{1x}, v_{2x} and v_{3x} denote the dislocation segment velocities along the direction perpendicular to the boundary that would result from the external force alone (see Section 4.3).

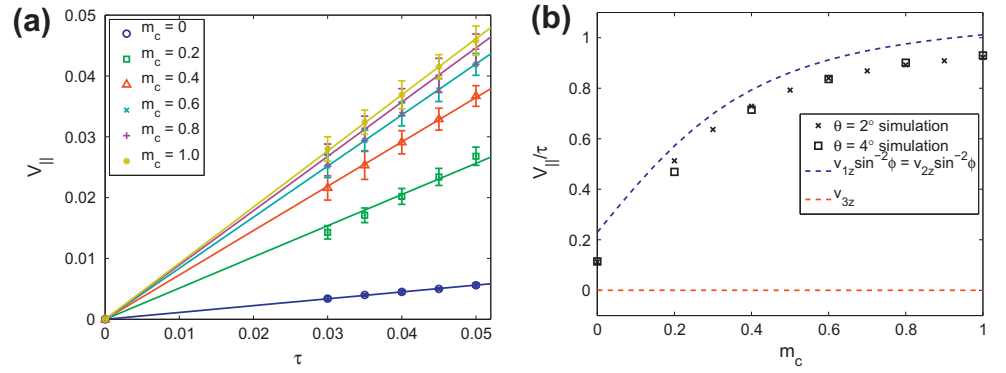

Fig. 7. (a) Steady-state (1 1 1)[1 1 0] LAMGB tangential velocity $V_\parallel$ (in units of $a\mu m_g$) (in the direction parallel to the $\left(\mathbf{b}_3, \hat{\boldsymbol{\xi}}_{r3}\right)$ mixed segment and along the boundary plane) as a function of the applied stress τ (in units of μ) for several values of dislocation climb mobility m_c (in units of m_g) at misorientation $\theta = 2.0°$. (b) The ratio of $V_\parallel$ to τ as a function of m_c for $\theta = 2.0°$ and $\theta = 4.0°$. Here, $v_{1z}\sin^{-2}\phi$, $v_{2z}\sin^{-2}\phi$ and v_{3z} again denote the dislocation segment velocities along the boundary plane that would result from the external force alone, corrected by the geometrical factor $\sin^2\phi$ (see Section 4.3).

since both $V_\perp$ and $V_\parallel$ are non-zero for finite values of τ at $m_c = 0$. $V_\perp$ and $V_\parallel$ are directly proportional to the applied stress τ. For positive values of τ, the migration velocity $V_\perp$ is always directed along $+\hat{\mathbf{x}}$, but the tangential velocity $V_\parallel$ switches direction from $+\hat{\mathbf{y}}$ to $-\hat{\mathbf{y}}$ at sufficiently high value for m_c. Figs. 4b and 5b in turn display the slope of $V_\perp$ vs. τ and $V_\parallel$ vs. τ, respectively, for two different values of the misorientation θ. These results show that both $V_\perp$ and $V_\parallel$ are independent of θ within the accuracy of our data.

For the (1 1 1)[1 1 0] boundary, the tangential velocity is parallel to the $\left(\mathbf{b}_3, \hat{\boldsymbol{\xi}}_{r3}\right)$ segment, i.e. $\mathbf{V}_\parallel = V_\parallel \hat{\mathbf{z}}$. The migration and tangential velocities, as a function of the applied stress $\tau = \sigma^0_{xy}$ for various values of dislocation climb mobility m_c and misorientation θ, are shown in Figs. 6 and 7, respectively. As with the (1 0 0)[1 1 0] boundary, the velocity data indicate that the (1 1 1)[1 1 0] boundary can migrate in a pure glide or a combined glide/climb mode, and that both $V_\perp$ and $V_\parallel$ for this boundary are proportional to τ and independent of θ within the accuracy of our data. However, in contrast to the (1 0 0)[1 10] boundary, where the tangential velocity changes sign with m_c, it is the migration velocity $V_\perp$ that changes sign with increasing m_c in the (1 1 1)[1 1 0] case. For positive values of τ, $V_\parallel$ in the (1 1 1)[1 1 0] boundary case is consistently directed along $+\hat{\mathbf{z}}$, but $V_\perp$ switches direction from $-\hat{\mathbf{x}}$ to $+\hat{\mathbf{x}}$ at sufficiently large values m_c.

The simulations show that the dislocation configurations during migration for both mixed boundaries examined in this work are very similar to their corresponding hexagonal networks observed in the absence of an externally applied stress (see Figs. 2 and 3). Hence, the migrating dislocation configuration may be approximated as a planar hexagonal network of straight dislocation segments, for which the velocity due to the driving force on each segment may be evaluated in order to determine how the dynamics of each segment in the hexagonal network influences the overall migration behavior of the boundary.

4. Analysis

4.1. Relaxation

As discussed in Section 3.1, both the (1 0 0)[1 1 0] and (1 1 1)[1 1 0] mixed boundaries are macroscopically flat (on the scale of a Burgers vector for the range of misorientations under consideration here) and may be approximated as a flat, hexagonal network of straight $\left(\mathbf{b}_1, \hat{\boldsymbol{\xi}}_{r1}\right)$, $\left(\mathbf{b}_2, \hat{\boldsymbol{\xi}}_{r2}\right)$ and $\left(\mathbf{b}_3, \hat{\boldsymbol{\xi}}_{r3}\right)$ dislocation segments, having a characteristic angle $\hat{\boldsymbol{\xi}}_{r1}\angle\hat{\boldsymbol{\xi}}_{r2} = 2\phi$. We can estimate the angle ϕ by balancing the elastic line tension between the dislocation segments that meet at each triple junction:

$$\mathscr{E}_3\hat{\boldsymbol{\xi}}_{r3} = \mathscr{E}_1\hat{\boldsymbol{\xi}}_{r1} + \mathscr{E}_2\hat{\boldsymbol{\xi}}_{r2}.$$

For a straight dislocation segment, the magnitude of the line tension is $\mathscr{E} = \frac{\alpha\mu}{4\pi}\log(R/r_0)\left[b^2_{\text{screw}} + b^2_{\text{edge}}/(1-\nu)\right]$ [28], where R is the simulation box size. Neglecting differences in the core energy and radius of different dislocation segments, the estimated values for ϕ are shown in Table 1. Comparison of the analytical results with those obtained from simulations shows errors less than 5% for the (1 0 0)[1 1 0] boundaries, and 11% for the (1 1 1)[1 1 0] boundaries.

4.2. Migration of (1 0 0)[1 1 0] boundaries

For the (1 0 0)[1 1 0] boundary, we approximate the dislocation configuration during steady-state migration as the hexagonal network shown in Fig. 1 with ϕ as per Table 1. For this boundary, the driving forces due to $\tau = \sigma^0_{xz}$ on the individual dislocation segments are (see Eq. (1)):

$$\mathbf{f}_1 = \frac{\tau}{2}\begin{pmatrix}\sin\phi\\ -\cos\phi\\ \sin\phi\end{pmatrix}, \quad \mathbf{f}_2 = \begin{pmatrix}f_{1x}\\ f_{1y}\\ -f_{1z}\end{pmatrix}, \quad \text{and} \quad \mathbf{f}_3 = \tau\begin{pmatrix}0\\ -1\\ 0\end{pmatrix}. \tag{5}$$

This shows that boundary migration (motion perpendicular to the boundary plane) is driven by the forces on segments $\left(\mathbf{b}_1, \hat{\boldsymbol{\xi}}_{r1}\right)$ and $\left(\mathbf{b}_2, \hat{\boldsymbol{\xi}}_{r2}\right)$. Although there is no force along the migration direction for the $\left(\mathbf{b}_3, \hat{\boldsymbol{\xi}}_{r3}\right)$ segment, this segment is dragged by the other two segments. The force analysis shows that the tangential motion of the boundary structure has contributions from all three dislocation segments. The total driving force on the boundary is (see Eqs. (C.1)–(C.3)):

$$\mathbf{F} = \begin{pmatrix}F_\perp\\ F_\parallel\\ 0\end{pmatrix} = \frac{\tau\theta}{\sqrt{2}}\begin{pmatrix}1\\ -1\\ 0\end{pmatrix}, \tag{6}$$

where $F_\perp$ and $F_\parallel$ are the driving forces for migration and tangential motion (along the y-direction), respectively.

Now, the velocities that would result from the external driving forces alone on the individual dislocation segments are given by (see Eqs. (2), (3) and (5)):

$$\mathbf{v}_1 = C_0\tau\begin{pmatrix}C_1m_g + C_2M_c\\ C_3m_g - C_4M_c\\ C_5m_g + C_6M_c\end{pmatrix}, \quad \mathbf{v}_2 = \begin{pmatrix}v_{1x}\\ v_{1y}\\ -v_{1z}\end{pmatrix},$$
$$\text{and} \quad \mathbf{v}_3 = m_g\tau\begin{pmatrix}0\\ -1\\ 0\end{pmatrix}, \tag{7}$$

where $M_c = [m_g^{-2} + (m_c^{-2} - m_g^{-2})\sin^2\alpha]^{-1/2}$ and $\alpha = \mathbf{b}_1\angle\hat{\boldsymbol{\xi}}_{r1} = \mathbf{b}_2\angle\hat{\boldsymbol{\xi}}_{r2} = \arccos[(\cos\phi + \sin\phi)/\sqrt{3}]$, with the coefficients $C_k(\phi)$ as given in Appendix D. The applied stress drives the $\left(\mathbf{b}_3, \hat{\boldsymbol{\xi}}_{r3}\right)$ screw segment to cross-slip, and induces the $\left(\mathbf{b}_1, \hat{\boldsymbol{\xi}}_{r1}\right)$ and $\left(\mathbf{b}_2, \hat{\boldsymbol{\xi}}_{r2}\right)$ mixed segments to glide as well as climb out of their respective slip planes.

In addition to the driving force, there are forces between the different segments such that the resulting motion of the boundary is a rigid translation of the constituent dislocation configuration. The velocity of the boundary $\mathbf{V}$ is equal to that of the dislocation triple junctions and the $\left(\mathbf{b}_3, \hat{\boldsymbol{\xi}}_{r3}\right)$ segment, but is related to the velocities of segments $\left(\mathbf{b}_1, \hat{\boldsymbol{\xi}}_{r1}\right)$ and $\left(\mathbf{b}_2, \hat{\boldsymbol{\xi}}_{r2}\right)$ by a geometric coupling factor. In particular, along the tangential direction (along y), the velocity of the dislocation triple junctions (and the boundary structure as a whole) is greater than that of segments $\left(\mathbf{b}_1, \hat{\boldsymbol{\xi}}_{r1}\right)$ and $\left(\mathbf{b}_2, \hat{\boldsymbol{\xi}}_{r2}\right)$ by a factor of $1/\cos^2\phi$. While it is not straightforward to account for all the internal forces between the dislocation segments in this simple theoretical analysis, it is still possible to explain the general features and trends observed in the simulation results of Figs. 4 and 5 using the velocities of individual dislocation segments in Eq. (7). First and foremost, the velocity of the boundary must be bounded by the fastest and slowest driven dislocation segments, i.e. $v_{3x} < V_\perp < v_{1x}$, and $v_{3y} < V_\parallel < v_{1y}\cos^{-2}\phi$. Since a rigid displacement of the boundary structure is observed in the simulations, the motion of the boundary must be limited by segments $\left(\mathbf{b}_1, \hat{\boldsymbol{\xi}}_{r1}\right)$ and $\left(\mathbf{b}_2, \hat{\boldsymbol{\xi}}_{r2}\right)$, which are driven to climb out of their respective slip planes. Therefore, it is not

Table 1
Comparison between simulation results and theoretical predictions for the characteristic angle $\hat{\boldsymbol{\xi}}_{r1}\angle\hat{\boldsymbol{\xi}}_{r2} = 2\phi$ of the hexagonal network.

Boundary	Simulation (°)	Theory (°)
(1 0 0)[1 1 0]	106.2	111.1
(1 1 1)[1 1 0]	97.77	88.72

unreasonable to expect that the resulting velocity of the boundary be comparable to the velocity of these segments:

$$V_\perp \lesssim v_{1x} = C_0(C_1 m_g + C_2 M_c)\tau \simeq (0.27 m_g + 0.15 M_c)\tau \quad (8)$$

and

$$V_\parallel \lesssim v_{1y}\cos^{-2}\phi = \cos^{-2}\phi C_0(C_3 m_g - C_4 M_c)\tau \simeq (0.12 m_g - M_c)\tau, \quad (9)$$

with the numerical factors obtained using the theoretical value of ϕ given in Table 1. Comparison between the simulation data and the analytical bounds displayed in Figs. 4b and 5b clearly shows that the boundary velocities extracted from the simulations are indeed bounded by the analytical expressions derived from the driven velocities of the dislocation segments. Furthermore, the simulation data is well approximated by the analytical upper bounds in Eqs. (8) and (9).

Interestingly, the migration of this boundary can occur simply by grain boundary dislocation glide, and hence the mobility is not dislocation-climb limited. The boundary is expected to migrate in the same direction as the driving force $F_\perp$, regardless of the temperature. In contrast to $V_\perp$, the tangential motion $V_\parallel$ of the boundary may be parallel or anti-parallel with respect to the driving force $F_\parallel$. At low values of m_c, $V_\parallel$ is anti-parallel to $F_\parallel$; in the limit that $m_c \to 0$, $V_\parallel \sim \cos^{-2}\phi C_0 C_3 m_g \tau \simeq 0.12 m_g \tau$ for $F_\parallel = -\tau\theta/\sqrt{2}$. For sufficiently large values of m_c, $V_\parallel$ switches direction so that it becomes parallel to $F_\parallel$. This implies that there exists a threshold climb mobility m_c^* (and correspondingly a threshold temperature T^*) at which $V_\parallel = 0$ and above (below) which it is (anti-)parallel to $F_\parallel$ even at constant $F_\parallel = -\tau\theta/\sqrt{2}$. Finally, we note that both $V_\perp$ and $V_\parallel$ are independent of the misorientation θ, in agreement with the simulation data.

4.3. Migration of (1 1 1)[1 1 0] boundaries

We analyze the migration of the (1 1 1)[1 1 0] boundary following a similar line of reasoning as in the case of the (1 0 0)[1 1 0] boundary. The driving forces due to $\tau = \sigma^0_{xy}$ on the individual segments of this boundary are:

$$\mathbf{f}_1 = \frac{\tau}{2\sqrt{3}}\begin{pmatrix}\cos\phi\\ -\sqrt{6}\cos\phi\\ \sqrt{6}\sin\phi\end{pmatrix}, \quad \mathbf{f}_2 = \begin{pmatrix}f_{1x}\\ -f_{1y}\\ f_{1z}\end{pmatrix},$$

$$\text{and} \quad \mathbf{f}_3 = \frac{\tau}{\sqrt{3}}\begin{pmatrix}1\\0\\0\end{pmatrix}. \quad (10)$$

This boundary migrates as a result of the driving forces on all segments, in contrast to the (1 0 0)[1 1 0] boundary (where the force along the direction perpendicular to the boundary on one of the segments is zero). Since there is no external driving force tangent to the boundary plane on the $\left(\mathbf{b}_3, \hat{\boldsymbol{\xi}}_{r3}\right)$ segment, it is carried along by the $\left(\mathbf{b}_1, \hat{\boldsymbol{\xi}}_{r1}\right)$ and $\left(\mathbf{b}_2, \hat{\boldsymbol{\xi}}_{r2}\right)$ segments as they move within the boundary plane. The total driving force on the boundary is (see Eqs. (C.1), (C.4) and (C.5)):

$$\mathbf{F} = \begin{pmatrix}F_\perp\\0\\F_\parallel\end{pmatrix} = \frac{\tau\theta}{\sqrt{3}}\begin{pmatrix}1\\0\\\sqrt{2}\end{pmatrix}, \quad (11)$$

where $F_\perp$ and $F_\parallel$ refer to the components of the driving force for migration and tangential motion (along the z-direction), respectively.

Next, we compute the velocities that would result from the external driving forces alone on the individual dislocation segments based on Eq. (10):

$$\mathbf{v}_1 = D_0\tau\begin{pmatrix}-D_1 m_g + D_2 M_c\\ D_3 m_g + D_4 M_c\\ D_5 m_g + D_6 M_c\end{pmatrix}, \quad \mathbf{v}_2 = \begin{pmatrix}v_{1x}\\ -v_{1y}\\ v_{1z}\end{pmatrix},$$

$$\text{and} \quad \mathbf{v}_3 = \frac{m_g\tau}{\sqrt{3}}\begin{pmatrix}1\\0\\0\end{pmatrix}, \quad (12)$$

where $M_c = \left[m_g^{-2} + (m_c^{-2} - m_g^{-2})\sin^2\alpha\right]^{-1/2}$ and $\alpha = \mathbf{b}_1\angle\hat{\boldsymbol{\xi}}_{r1} = \mathbf{b}_2\angle\hat{\boldsymbol{\xi}}_{r2} = \arccos\left[\sqrt{2}(\cos\phi + \sqrt{3}\sin\phi)/3\right]$, with the coefficients $D_k(\phi)$ as given in Section D.

The applied stress drives the $\left(\mathbf{b}_3, \hat{\boldsymbol{\xi}}_{r3}\right)$ mixed segment to glide in its slip plane, but yields both glide and climb forces on the $\left(\mathbf{b}_1, \hat{\boldsymbol{\xi}}_{r1}\right)$ and $\left(\mathbf{b}_2, \hat{\boldsymbol{\xi}}_{r2}\right)$ mixed segments. Nevertheless, these segments are held in place relative to one another by internal forces between the segments so that the boundary undergoes a rigid translation at a steady-state velocity under a constant applied stress.

As in the (1 0 0)[1 1 0] boundary case, the general features and trends of simulation results for this boundary, displayed in Figs. 6 and 7, may be understood by considering the velocities of individual dislocation segments, Eq. (12). The tangential velocity (along z) of the dislocation triple junctions (and overall boundary structure) is greater than that for the $\left(\mathbf{b}_1, \hat{\boldsymbol{\xi}}_{r1}\right)$ and $\left(\mathbf{b}_2, \hat{\boldsymbol{\xi}}_{r2}\right)$ segments by a factor of $1/\sin^2\phi$. The velocity of this boundary is bounded by the fastest and slowest individual segments, such that $v_{1x} < V_\perp < v_{3x}$, and $v_{3z} < V_\parallel < v_{1z}\sin^{-2}\phi$, and is expected to be comparable with the velocity of segments $\left(\mathbf{b}_1, \hat{\boldsymbol{\xi}}_{r1}\right)$ and $\left(\mathbf{b}_2, \hat{\boldsymbol{\xi}}_{r2}\right)$, which are driven to climb out of their respective slip planes:

$$V_\perp \gtrsim v_{1x} = D_0(-D_1 m_g + D_2 M_c)\tau \simeq (-0.21 m_g + 0.42 M_c) \quad (13)$$

and

$$V_\parallel \lesssim v_{1z}\sin^{-2}\phi = \sin^{-2}\phi D_0(D_5 m_g + D_6 M_c)\tau \simeq (0.23 m_g + 0.78 M_c)\tau. \quad (14)$$

The numerical factors in these expressions were obtained by setting $\phi = 88.7°$ (see Table 1). Comparison between the simulation data and the analytical bounds displayed in Figs. 6b and 7b clearly shows that the boundary velocities extracted from the simulations are indeed bounded by the analytical expressions. The analytical bounds associated with segments $\left(\mathbf{b}_1, \hat{\boldsymbol{\xi}}_{r1}\right)$ and $\left(\mathbf{b}_2, \hat{\boldsymbol{\xi}}_{r2}\right)$ closely match the boundary velocities determined from the simulations.

As in the case of the (1 0 0)[1 1 0] boundary, our analysis and numerical simulations indicate that the motion of the (1 1 1)[1 1 0] boundary is not dislocation-climb limited, and can switch directions as the climb mobility is varied. For this boundary, however, the tangential motion $V_{\parallel}$ is always in the direction of the driving force $F_{\parallel}$, while its migration $V_{\perp}$ displays an intriguing switch in sign upon varying m_c. In particular, $V_{\perp}$ is anti-parallel to $F_{\perp}$ for low values of m_c; in the limit that $m_c \to 0$, $V_{\perp} \sim -\sin^{-2}\phi\, D_0 D_1 m_g \tau \simeq -0.21 m_g \tau$ for $F_{\perp} = \tau\theta/\sqrt{3}$, and so the boundary migrates in the direction opposite to the driving force $F_{\perp}$. On the other hand, for sufficiently large values of m_c, $V_{\perp}$ is parallel to $F_{\perp}$. This again implies that there exists a threshold climb mobility value m_c^* (and correspondingly a threshold temperature T^*) at which $V_{\perp} = 0$ and above (below) which it is (anti-) parallel to $F_{\perp}$ for constant $F_{\perp} = \tau\theta/\sqrt{3}$. Again, we note that both $V_{\perp}$ and $V_{\parallel}$ are independent of the misorientation θ, in agreement with the simulation data.

5. Discussion

We have presented the first systematic investigation of stress-induced migration of LAMGBs using a three-dimensional discrete dislocation dynamics simulation method which accounts for both topological changes in the dislocation network and dislocation reactions. As described in Section 2, the mixed boundaries were constructed from two sets of intersecting lattice dislocations having mixed edge/screw character. Within each set, dislocation lines were initially straight and uniformly spaced. The two mixed boundaries were represented initially by bcc lattice dislocations, i.e. $\frac{a}{2}\langle 1\,1\,1\rangle$ dislocations in the $\{1\,1\,0\}$ slip planes. Each of these boundaries represents a broader class of mixed boundaries corresponding to $\hat{\boldsymbol{v}} \cdot (\mathbf{b}_1 \pm \mathbf{b}_2) = 0$, respectively. Upon relaxation, dislocation reactions at the intersections lead to approximately planar hexagonal dislocation networks, as observed in experiments [30].

The motion of such boundaries was investigated as a function of the applied stress for several values of dislocation climb to glide mobility ratios and misorientation angles. Under an applied shear stress that provides the driving force for boundary migration, the hexagonal dislocation network was found to undergo a rigid translation along directions perpendicular and parallel to the boundary plane. The migration of a mixed boundary can occur by dislocation glide, and necessarily couples to the tangential motion (parallel to the boundary plane) because the applied stress that gives rise to boundary migration also generates a force on the dislocation network parallel to the boundary plane. The tangential motion of the grain boundary dislocations having a net Burgers vector in the plane of the boundary is expected to induce grain boundary sliding, while the migration of the boundary is expected to produce shear deformation (arising from the tilt character of boundary) and rotation (arising from the twist character of boundary) of the crystal lattice within the region traversed by the migrating boundary [5,16,31].

In the analysis presented in Section 4, we obtained theoretical estimates for the configurational parameters and the translation velocity of the dislocation network of these LAMGBs. Under the applied stresses that drive boundary migration, two of the dislocation segments that make up the dislocation array, i.e. $\left(\mathbf{b}_1, \hat{\boldsymbol{\xi}}_{r1}\right)$ and $\left(\mathbf{b}_2, \hat{\boldsymbol{\xi}}_{r2}\right)$, are forced to climb out of their respective slip planes as they glide, while one of the dislocation segments, i.e. $\left(\mathbf{b}_3, \hat{\boldsymbol{\xi}}_{r3}\right)$, can move by pure glide. Although the segments are driven to move at different velocities, every segment within the boundary moves with the same (i.e. boundary) velocity at steady-state; this occurs through the internal forces between segments. While the internal forces between the segments are a priori unknown and not easily evaluated analytically, rigorous bounds on the grain boundary velocity were obtained. The bound associated with the climbing dislocation segments provides a good estimate of the boundary velocity as a function of the applied stress, dislocation climb mobility and misorientation.

Our simulations and theoretical analyses show that the migration and tangential velocities of each boundary are directly proportional to the applied stress and independent of the misorientation θ. In general, we expect that the dependence of the grain boundary velocity $\mathbf{V}$ on the driving force $\mathbf{F}$ is given by $\mathbf{V} = \mathbb{M}_{GB} \cdot \mathbf{F}$, where $\mathbb{M}_{GB}$ denotes the grain boundary mobility tensor. Given that $\mathbf{V}$ is independent of θ and that $\mathbf{F}$ is proportional to θ as per Eqs. (6) and (11), this implies that the grain boundary mobility tensor is inversely proportional to θ, i.e. $\mathbb{M}_{GB} \sim \theta^{-1}$. Furthermore, $\mathbb{M}_{GB}$ is expected to be both positive definite and symmetric (as per Onsager's reciprocity relations), and depend only on the constituent dislocation structure of the boundary. In three spatial dimensions, $\mathbb{M}_{GB}$ contains six independent components, which may be found by evaluating $\mathbf{V}$ arising from each component of $\mathbf{F}$ separately. However, it can be seen from Eqs. (C.2) and (C.4) that the components of the driving force $\mathbf{F}$ for boundary motion due to the external stress $\boldsymbol{\sigma}^0$ cannot be independently varied to resolve each and every element of $\mathbb{M}_{GB}$; indeed, as shown in Eqs. (C.3) and (C.5), the applied stress τ that generates boundary migration also induces a non-zero driving force parallel to the boundary plane. Nevertheless, we may evaluate the effective mobilities $\mathscr{M}_{\perp} = V_{\perp}/\tau$ and

$\mathscr{M}_{\parallel} = V_{\parallel}/\tau$, each of which is a linear combination of the components of $\mathbb{M}_{GB}$.

To this end, based on the values of the dislocation glide mobility in bcc Mo obtained from molecular dynamics simulations at 300 K [29], the magnitude of the effective mobility for migration $\mathscr{M}_{\perp}$ at temperatures for which $m_c \ll m_s \approx m_g$ (unlike m_c and m_s, m_g does not vary substantially with temperature) may be estimated to be $0.46\ \mathrm{m\,s^{-1}\,MPa^{-1}}$ and $0.37\ \mathrm{m\,s^{-1}\,MPa^{-1}}$ for mixed boundaries (1 0 0)[1 1 0] and (1 1 1)[1 1 0], respectively. Intriguingly, our simulations of the migration of (1 1 1)[1 1 0] boundaries also showed that the direction of grain boundary migration depends on the dislocation climb mobility (temperature). In addition, the tangential component of the velocity of some boundaries (e.g. the (1 0 0)[1 1 0] boundaries here) may also depend on dislocation climb mobility and hence temperature. Thus, the direction of boundary displacement may be controlled by temperature, and to a lesser extent, the constituent dislocation structure.

The switch in the sign for the grain boundary velocity arises from the competition between dislocation glide and climb. If the contributions associated with glide and climb are opposite in sign, then a switch in the sign for the velocity may be observed at sufficiently high temperature. Theoretically, we can anticipate switch-over for each velocity component and approximate the threshold dislocation climb mobility m_c^* (and hence temperature T^*), for which the change in direction occurs by solving for the value of m_c when $V_{\perp} = 0$ and $V_{\parallel} = 0$ within the theoretical framework established in Section 4. If $0 < m_c^* \ll m_g$, then there exists a possibility that the switch in sign for the boundary migration or tangential velocity may be observed under experimentally relevant conditions.

Geometrically, the switch in the sign for the migration or tangential velocities may be understood by considering Fig. 8. First, we note that all simple LAMGBs studied here are not dislocation-climb limited, i.e. $V_{\perp}$ and $V_{\parallel}$ are both finite at $m_c = 0$ when $\mathbf{F} \neq 0$. Furthermore, the boundary velocity for $m_c = 0$, $\mathbf{V}(m_c = 0)$, is in general misaligned with respect to the driving force $\mathbf{F}$. Now, as m_c gradually increases from zero, $\mathbf{V}$ tends to rotate towards $\mathbf{F}$, i.e. the boundary mobility tends to become more isotropic. The switch in sign for either the migration or tangential component of $\mathbf{V}$ will depend on the orientation of the boundary plane relative to the boundary velocity $\mathbf{V}$ at $m_c = m_g$, $\mathbf{V}(m_c = m_g)$, and the boundary velocity $\mathbf{V}$ at zero climb. If the boundary plane lies between $\mathbf{V}(m_c = m_g)$ and $\mathbf{V}(m_c = 0)$, as shown in Fig. 8a, the switch in sign can occur for the migration component of $\mathbf{V}$. On the other hand, if the normal to the boundary plane $\hat{\boldsymbol{\nu}}$ lies between $\mathbf{V}(m_c = m_g)$ and $\mathbf{V}(m_c = 0)$, as shown in Fig. 8b, then the switch in sign can occur for the tangential component of $\mathbf{V}$. Finally, if $\mathbf{V}(m_c = m_g)$ and $\mathbf{V}(m_c = 0)$ both lie between the boundary plane and its normal, then no switch in sign for any velocity component is expected to occur. It should be noted that for an arbitrary (as opposed to simple) LAMGB, $\mathbf{V}(m_c = 0)$ may assume a direction that is either parallel (perpendicular) to the grain boundary. In such cases, the migration (tangential) velocity is dislocation-climb controlled, and no switching behavior is expected to occur.

To make the above discussion more concrete, consider a broader class of simple LAMGBs in a bcc crystal, which may be described by two sets of equally spaced, intersecting $\frac{a}{2}\langle 1\,1\,1\rangle$ -type dislocations, and which subsequently react to form a $a\langle 1\,0\,0\rangle$-type segment. Employing the theoretical framework in Section 4, a systematic sampling of 1536 fundamental boundary plane orientations relative to the Burgers vector pairs that make up the mixed boundary, i.e. $\mathbf{b}_1, \mathbf{b}_2 \in \frac{a}{2}\langle 1\,1\,1\rangle$ and the corresponding boundary plane normals $\hat{\boldsymbol{\nu}}$ consistent with $\hat{\boldsymbol{\nu}} \cdot (\mathbf{b}_1 \pm \mathbf{b}_2) = 0$, confirms that the $\mathbf{b}_1$ and $\mathbf{b}_2$ segments are in general driven to simultaneously glide and climb, while the $\mathbf{b}_3 = \mathbf{b}_1 + \mathbf{b}_2$ segment is driven to glide (or cross-slip if it is a screw segment) under an applied stress that induces the migration of the boundary. Examination of the driving force on segment $\mathbf{b}_1$ (or $\mathbf{b}_2$) for every orientation of the boundary plane in the ensemble indicates that a change in sign for the migration or tangential translation is not specific to the (1 0 0)[1 1 0] or (1 1 1)[1 1 0] mixed boundaries we have simulated, but is a general feature that applies to most such mixed boundaries. In the case of $\hat{\boldsymbol{\nu}} \cdot (\mathbf{b}_1 + \mathbf{b}_2) = 0$, the change in sign

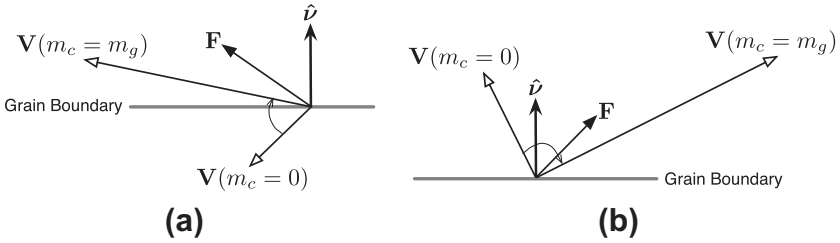

Fig. 8. Schematic representation of the geometrical relationship between boundary velocity $\mathbf{V}$ at zero and non-zero climb mobilities, the driving force $\mathbf{F}$ for boundary motion, and the boundary plane that gives rise to the switch in sign for (a) migration and (b) tangential components of the boundary velocity $\mathbf{V}$. If $\mathbf{V}(m_c = 0)$ and $\mathbf{V}(m_c = m_g)$ both lie between the boundary plane and its normal, then no switch in sign for any velocity component is expected to occur. Note that even when $m_c \to m_g$, $\mathbf{V}$ in general is not parallel to $\mathbf{F}$, i.e. while the mobility tensor for the individual dislocation segments becomes isotropic, the grain boundary mobility tensor remains anisotropic.

for tangential motion occurs for 70% of the boundaries at $2.6 \times 10^{-4} \lesssim m_c^*/m_g \lesssim 0.21$. On the other hand, the change in sign for migration is a generic feature occurring at $0.22 \lesssim m_c^*/m_g \lesssim 0.27$ for all boundaries in the ensemble such that $\hat{\mathbf{v}} \cdot (\mathbf{b}_1 - \mathbf{b}_2) = 0$.

In practice, the predicted value of m_c^*/m_g may be much larger than the range of values realizable under typical experimental conditions, as is the case with the prototypical (1 0 0)[1 1 0] and (1 1 1)[1 1 0] LAMGBs. Although the actual change in sign for the boundary velocity may not be directly observable, our finding has important consequences for interpreting experimental measurements of grain boundary mobility for such boundaries. For example, changing the temperature will lead to changes in both the dislocation glide and climb mobility, and hence the ratio of these two mobilities. This implies that the boundary mobility will not, in general, be a simple Arrhenius function, but will have contributions from the activation energies of both the dislocation climb and glide mobilities.

In the work of Gorkaya et al. [5], the grain boundary misorientation decreases during the stress-induced boundary migration. This occurs because finite-sized grains rotate by expelling dislocations through the free surfaces in these experiments. In the present simulations, the grain boundary structure is periodic such that no free surfaces are present; hence, no dislocations can be expelled and there can be no misorientation change. However, based upon the results presented above, we can evaluate the influence of such changes in misorientation on stress-driven boundary migration in finite-sized grains. The simulations and analysis show that the grain boundary migration velocity $V_\perp$ is independent of misorientation and hence will not change if dislocations were expelled (as long as the structure of the dislocation network is preserved). However, the driving force for boundary migration $F_\perp$ scales proportionally to the misorientation θ and will therefore change if dislocations are expelled. This implies that if θ decreases during boundary migration, the boundary mobility will increase as $1/\theta$. While the present simulations say nothing about dislocation egress through a free surface, a qualitative sense of that rate may be deduced from the tangential velocity of the dislocation structure that makes up the grain boundary.

Finally, in the present work, the boundaries were also assumed to be free of impurities and "extrinsic" or redundant dislocations that are not geometrically necessary (and thus do not contribute to the overall misorientation of the boundary). Previously, we have shown, both numerically and analytically, that the presence of such extrinsic dislocations can significantly alter the mobility of simple low-angle tilt boundaries [3]. Similarly, it is well known that the interaction of grain boundaries with solutes can also significantly alter boundary mobility [32–36]. The analytical framework employed in this work can be used to quantitatively assess these effects on grain boundary mobility. While the present approach is limited to low-angle grain boundaries, it does allow for a much more mechanistic and structurally aware understanding of boundary migration than is possible for high-angle boundaries, where the boundary structure is much more complex (and boundary motion is not easily describable in terms of discrete dislocation dynamics), and for which the coupling of externally applied stress to the boundary structure is not known.

6. Conclusion

Dislocation dynamics simulations and theoretical analyses of the stress-driven migration of LAMGBs have been employed to provide a detailed understanding of the influence of grain boundary structure on boundary motion. Unless impeded by other crystal defects such as impurities and extrinsic dislocations, simple LAMGBs can move by dislocation glide. Concomitant with the stress-induced migration of such boundaries is the motion parallel to the boundary plane. The results presented here showed an intriguing reversal in the direction of boundary migration or tangential motion as a function of dislocation climb mobility, and hence, temperature. Theoretical analysis of over 1500 grain boundaries suggests that this type of phenomena is general for this class of boundaries.

Appendix A. Construction of LAMGBs

Whereas a simple low-angle symmetric tilt boundary may be constructed using just one set of dislocations, a LAMGB must contain at least two sets of intersecting dislocations [2]. In the present study, we modeled LAMGBs using two sets of straight dislocations $\left(\mathbf{b}_1, \hat{\boldsymbol{\xi}}_1\right)$ and $\left(\mathbf{b}_2, \hat{\boldsymbol{\xi}}_2\right)$ that are uniformly spaced with line spacings D_1 and D_2, respectively. The intersecting dislocation lines uniquely define the boundary plane, which is perpendicular to the boundary normal vector:

$$\hat{\mathbf{v}} = \frac{\hat{\boldsymbol{\xi}}_1 \times \hat{\boldsymbol{\xi}}_2}{\left|\hat{\boldsymbol{\xi}}_1 \times \hat{\boldsymbol{\xi}}_2\right|}. \tag{A.1}$$

For such a dislocation array to represent a grain boundary, it must be free of long-range stresses. This is achieved by relating the parameters of the dislocation array (such as the Burgers vector, dislocation line direction, and dislocation spacing of each set) to the five macroscopic degrees of freedom for a grain boundary through Frank's formula. For example, the dislocation line directions must be related to the Burgers vectors and boundary plane normal $\hat{\mathbf{v}}$ as follows:

$$\hat{\boldsymbol{\xi}}_1 = \frac{\mathbf{b}_2 \times \hat{\mathbf{v}}}{|\mathbf{b}_2 \times \hat{\mathbf{v}}|} \quad \text{and} \quad \hat{\boldsymbol{\xi}}_2 = \frac{\hat{\mathbf{v}} \times \mathbf{b}_1}{|\hat{\mathbf{v}} \times \mathbf{b}_1|}. \tag{A.2}$$

If this condition is satisfied, then the dislocation array represents a boundary between grains that are misoriented about the axis:

$$\hat{\mathbf{u}} = \frac{\mathbf{b}_1 \times \mathbf{b}_2}{|\mathbf{b}_1 \times \mathbf{b}_2|}, \tag{A.3}$$

at an angle that is inversely proportional to the dislocation spacing in each set:

$$\theta = \frac{|\mathbf{b}_1 \times \mathbf{b}_2|}{|\mathbf{b}_2 \times \hat{\mathbf{v}}|} \cdot \frac{1}{D_1} = \frac{|\mathbf{b}_1 \times \mathbf{b}_2|}{|\hat{\mathbf{v}} \times \mathbf{b}_1|} \cdot \frac{1}{D_2}. \tag{A.4}$$

As the above procedure is equally valid for a twist boundary, the Burgers vectors and line directions of dislocations used to construct a mixed boundary must be judiciously chosen so that the boundary has both twist and tilt character, i.e. $\hat{\mathbf{v}}$ is neither parallel nor perpendicular to $\hat{\mathbf{u}}$. If the angle between $\hat{\mathbf{v}}$ and $\hat{\mathbf{u}}$ is χ, the extent of twist character may be specified in terms of the deviation of $\hat{\mathbf{v}}$ from pure tilt character, i.e. $\pi/2 - \chi$; this is also known as the "twist angle" [5]. Alternatively, the fraction of twist and tilt character for a mixed boundary may be determined by resolving $\hat{\mathbf{v}}$ into twist ($\cos\chi$) and tilt ($\sin\chi$) components and making use of the trigonometric identity $\sin^2\chi + \cos^2\chi \equiv 1$. Therefore, the fraction of twist and tilt for a mixed boundary may be determined as $\cos^2\chi$ and $\sin^2\chi$, respectively. Both descriptions are employed.

In the present study, we focus on simple LAMGBs, for which the magnitude of the lattice Burgers vectors and dislocation spacing in each set are equal, i.e. $b_1 = b_2 = b$ and $D_1 = D_2 = D$. In this case, Eq. (A.4) yields $|\mathbf{b}_2 \times \hat{\mathbf{v}}| = |\hat{\mathbf{v}} \times \mathbf{b}_1|$. This implies that $\sin\kappa_2 = \sin\kappa_1$, where κ_1 and κ_2 are the angles between $\hat{\mathbf{v}}$ with $\mathbf{b}_1$ and $\mathbf{b}_2$, respectively. Hence, $\kappa_2 = \kappa_1$ or $\kappa_2 = \pi - \kappa_1$ and this implies Eq. (4).

Hence, once the Burgers vectors $\mathbf{b}_1$ and $\mathbf{b}_2$ are chosen, Eqs. (A.1), (A.2) and (4) are employed to determine the dislocation line directions $\hat{\boldsymbol{\xi}}_1$ and $\hat{\boldsymbol{\xi}}_2$, and the boundary plane normal $\hat{\mathbf{v}}$ self-consistently. The restrictions on the parameters of the constituent dislocations imply that the boundary normal must be perpendicular to either $\mathbf{b}_1 + \mathbf{b}_2$, or $\mathbf{b}_1 - \mathbf{b}_2$. It should be noted that $\hat{\mathbf{v}}$ cannot simultaneously fulfill both conditions; otherwise the boundary loses its mixed character and becomes a pure twist boundary, since $\hat{\mathbf{v}} \| \mathbf{b}_1 \times \mathbf{b}_2$ implies $\hat{\mathbf{v}} \| \hat{\mathbf{u}}$ by Eq. (A.3).

Appendix B. Simulation geometry

Regardless of the combination of $\frac{a}{2}\langle 1\,1\,1\rangle$ Burgers vectors chosen, the boundaries can be constructed to have the same orientation within the simulation box. To ensure that the boundary is parallel to the yz-plane of the rectangular parallelepiped simulation cell, the simulation coordinate system is defined as follows:

$$\hat{\mathbf{x}} = \hat{\mathbf{v}} = \frac{\hat{\boldsymbol{\xi}}_1 \times \hat{\boldsymbol{\xi}}_2}{\left|\hat{\boldsymbol{\xi}}_1 \times \hat{\boldsymbol{\xi}}_2\right|}, \quad \hat{\mathbf{y}} = \frac{\hat{\boldsymbol{\xi}}_1 - \hat{\boldsymbol{\xi}}_2}{\left|\hat{\boldsymbol{\xi}}_1 - \hat{\boldsymbol{\xi}}_2\right|}, \quad \text{and} \quad \hat{\mathbf{z}} = \frac{\hat{\boldsymbol{\xi}}_1 + \hat{\boldsymbol{\xi}}_2}{\left|\hat{\boldsymbol{\xi}}_1 + \hat{\boldsymbol{\xi}}_2\right|}.$$

In this coordinate system, the dislocation line directions have reflection symmetry about $\hat{\mathbf{z}}$ and may be written as:

$$\hat{\boldsymbol{\xi}}_1 = \begin{bmatrix} 0 & \xi_y & \xi_z \end{bmatrix} \quad \text{and} \quad \hat{\boldsymbol{\xi}}_2 = \begin{bmatrix} 0 & -\xi_y & \xi_z \end{bmatrix}, \tag{B.1}$$

with $\xi_y > 0$ and $\xi_z > 0$. The periodicity of the lozenge network is L_y and L_z along the $\hat{\mathbf{y}}$ and $\hat{\mathbf{z}}$, respectively, such that:

$$\frac{L_y}{L_z} = \frac{\xi_{1y}}{\xi_{1z}}. \tag{B.2}$$

Using Eqs. (A.2), (A.3), (B.1) and (B.2), we find that:

$$b_{1y} L_y = b_{1z} L_z,$$

and that the components of $\mathbf{b}_1$ and $\mathbf{b}_2$ are related as follows: $b_{2x} = \pm b_{1x}$, $b_{2y} = -b_{1y}$, and $b_{2z} = b_{1z}$. Consequently, if:

$$\mathbf{b}_1 = \begin{bmatrix} b_x & b_y & b_z \end{bmatrix}, \quad \text{where} \quad b_x \neq 0 \quad \text{and}$$
$$b_z = \frac{L_y}{L_z} b_y \neq 0, \tag{B.3}$$

$\mathbf{b}_2$ and $\mathbf{b}_3$ have the following components:

$$\mathbf{b}_2 = \begin{cases} \begin{bmatrix} -b_x & -b_y & b_z \end{bmatrix} & \text{if } \hat{\mathbf{v}} \cdot (\mathbf{b}_1 + \mathbf{b}_2) = b_{1x} + b_{2x} = 0 \\ \begin{bmatrix} b_x & -b_y & b_z \end{bmatrix} & \text{if } \hat{\mathbf{v}} \cdot (\mathbf{b}_1 - \mathbf{b}_2) = b_{1x} - b_{2x} = 0 \end{cases}, \tag{B.4}$$

$$\mathbf{b}_3 = \begin{cases} 2\begin{bmatrix} 0 & 0 & b_z \end{bmatrix} & \text{if } \hat{\mathbf{v}} \cdot (\mathbf{b}_1 + \mathbf{b}_2) = b_{1x} + b_{2x} = 0 \\ 2\begin{bmatrix} b_x & 0 & b_z \end{bmatrix} & \text{if } \hat{\mathbf{v}} \cdot (\mathbf{b}_1 - \mathbf{b}_2) = b_{1x} - b_{2x} = 0 \end{cases}. \tag{B.5}$$

Regardless of the orientation of the boundary plane, it can be shown from Eqs. (B.1), (B.3) and (B.4) that $\mathbf{b}_1 \cdot \hat{\boldsymbol{\xi}}_1 = \mathbf{b}_2 \cdot \hat{\boldsymbol{\xi}}_2$, which means that dislocation $\left(\mathbf{b}_1, \hat{\boldsymbol{\xi}}_1\right)$ has the same character angle as dislocation $\left(\mathbf{b}_2, \hat{\boldsymbol{\xi}}_2\right)$; the character angle for $\mathbf{b}_1$ and $\mathbf{b}_2$ varies from one boundary to another. When these react in the boundary to form $\left(\mathbf{b}_1, \hat{\boldsymbol{\xi}}_{r1}\right)$, $\left(\mathbf{b}_2, \hat{\boldsymbol{\xi}}_{r2}\right)$ and $\left(\mathbf{b}_3, \hat{\boldsymbol{\xi}}_{r3}\right)$ dislocation segments, the resulting dislocation line directions will once again have reflection symmetry about $\hat{\mathbf{z}}$:

$$\hat{\boldsymbol{\xi}}_{r1} = \begin{bmatrix} 0 & \xi_{ry} & \xi_{rz} \end{bmatrix}, \quad \hat{\boldsymbol{\xi}}_{r2} = \begin{bmatrix} 0 & -\xi_{ry} & \xi_{rz} \end{bmatrix}, \quad \text{and}$$
$$\hat{\boldsymbol{\xi}}_{r3} = \hat{\mathbf{z}} = [0\ 0\ 1], \tag{B.6}$$

with $\xi_{ry} > 0$ and $\xi_{rz} > 0$. From Eqs. (B.3)–(B.6), it can similarly be shown that $\left(\mathbf{b}_1, \hat{\boldsymbol{\xi}}_{r1}\right)$ will also have the same character angle as $\left(\mathbf{b}_2, \hat{\boldsymbol{\xi}}_{r2}\right)$, while $\left(\mathbf{b}_3, \hat{\boldsymbol{\xi}}_{r3}\right)$ is a pure screw segment for $\hat{\mathbf{v}} \cdot (\mathbf{b}_1 + \mathbf{b}_2) = 0$, but a mixed segment for $\hat{\mathbf{v}} \cdot (\mathbf{b}_1 - \mathbf{b}_2) = 0$. Finally, the straight length segments of $\left(\mathbf{b}_1, \hat{\boldsymbol{\xi}}_{r1}\right)$, $\left(\mathbf{b}_2, \hat{\boldsymbol{\xi}}_{r2}\right)$ and $\left(\mathbf{b}_3, \hat{\boldsymbol{\xi}}_{r3}\right)$ within the hexagonal network, which we denote as L_1, L_2 and L_3, respectively, can be found by setting $L_1 = L_2$ due to symmetry considerations, and noting that the configuration must fit within the dimensions of the unit cell $L_y \times L_z$, which remains the same before and after reaction:

$$L_1 = L_2 = \frac{1}{2}\frac{L_y}{\xi_{ry}} \quad \text{and} \quad L_3 = \frac{1}{2}\left(L_z - L_y \frac{\xi_{rz}}{\xi_{ry}}\right).$$

Appendix C. Migration of simple LAMGBs induced by stress

To find the stress tensor components that couple to the migration of a simple LAMGB, we consider the most gen-

eral form for the externally applied stress $\boldsymbol{\sigma}^0$ and denote the Peach–Kohler force on segments $\left(\mathbf{b}_1, \hat{\boldsymbol{\xi}}_{r1}\right)$, $\left(\mathbf{b}_2, \hat{\boldsymbol{\xi}}_{r2}\right)$ and $\left(\mathbf{b}_3, \hat{\boldsymbol{\xi}}_{r3}\right)$ to be $\mathbf{f}_1$, $\mathbf{f}_2$ and $\mathbf{f}_3$, respectively. From a mechanistic perspective, a boundary moves when subjected to the applied stress $\boldsymbol{\sigma}^0$ due to a driving force per unit area:

$$\mathbf{F} = \frac{2(\mathbf{f}_1 L_1 + \mathbf{f}_2 L_2 + \mathbf{f}_3 L_3)}{L_y L_z}, \tag{C.1}$$

with the force for migration $F_\perp$ being the component of $\mathbf{F}$ perpendicular to the boundary plane (the x-direction in our case). For each set of boundaries considered here, it will be shown that there is only one component of $\boldsymbol{\sigma}^0$ that gives a non-zero $F_\perp$.

For the boundary plane determined by $\hat{\boldsymbol{v}} \cdot (\mathbf{b}_1 + \mathbf{b}_2) = 0$, the boundary moves due to the driving force:

$$\mathbf{F} = \frac{2}{L_z}\begin{pmatrix} -\sigma^0_{xz} b_x \\ -\sigma^0_{xz} b_y \\ \sigma^0_{xx} b_x + \sigma^0_{xy} b_y \end{pmatrix}. \tag{C.2}$$

This implies that the boundary migrates under the stress component $\sigma^0_{xz} = \sigma^0_{zx}$, for which the Peach–Kohler forces on the segments normal to the boundary plane are: $f_{1x} = f_{2x} = -\sigma^0_{xz} b_x \xi_{ry}$ and $f_{3x} = 0$, and which result in a net driving force:

$$\mathbf{F} = \begin{pmatrix} F_\perp \\ F_\parallel \\ 0 \end{pmatrix} = -\frac{2\sigma^0_{xz}}{L_z}\begin{pmatrix} b_x \\ b_y \\ 0 \end{pmatrix}. \tag{C.3}$$

We note that the force on segment $\left(\mathbf{b}_3, \hat{\boldsymbol{\xi}}_{r3}\right)$ normal to the boundary plane vanishes. This implies that the other two segments must "drag" the third one in order for the boundary to migrate.

On the other hand, for the boundary plane determined by $\hat{\boldsymbol{v}} \cdot (\mathbf{b}_1 - \mathbf{b}_2) = 0$, the driving force on the boundary arising from the applied stress $\boldsymbol{\sigma}^0$ is:

$$\mathbf{F} = \frac{2}{L_y}\begin{pmatrix} \sigma^0_{xy} b_x \\ -\sigma^0_{xx} b_x - \sigma^0_{xz} b_z \\ \sigma^0_{xy} b_z \end{pmatrix}. \tag{C.4}$$

Therefore, the boundary migrates under the stress component $\sigma^0_{xy} = \sigma^0_{yx}$, for which the Peach–Kohler forces on the segments normal to the boundary plane are $f_{1x} = f_{2x} = \sigma^0_{xy} b_x \xi_{rz}$ and $f_{3x} = 2\sigma^0_{xy} b_x$, and which result in a net driving force

$$\mathbf{F} = \begin{pmatrix} F_\perp \\ 0 \\ F_\parallel \end{pmatrix} = \frac{2\sigma^0_{xy}}{L_y}\begin{pmatrix} b_x \\ 0 \\ b_z \end{pmatrix}. \tag{C.5}$$

In contrast to the first case, the external stress now gives rise to non-zero driving forces normal to the boundary plane for all the dislocation segments.

Appendix D. Coefficients $C_k(\phi)$ and $D_k(\phi)$

The coefficients C_k and D_k for the driven velocities of segments $\left(\mathbf{b}_1, \hat{\boldsymbol{\xi}}_{r1}\right)$ and $\left(\mathbf{b}_2, \hat{\boldsymbol{\xi}}_{r2}\right)$ for the (1 0 0)[1 1 0] and (1 1 1)[1 1 0] LAMGBs, respectively, are as follows:

$$\begin{aligned}
C_0 &= [4(2-\sin 2\phi)]^{-1} & D_0 &= [6\sqrt{2}(5+2\cos 2\phi - 2\sqrt{3}\sin 2\phi)]^{-1} \\
C_1 &= 2\cos\phi & D_1 &= \sqrt{2}(5\sqrt{3}\cos\phi - 6\sin\phi) \\
C_2 &= -3\cos\phi + \cos 3\phi + 4\sin\phi & D_2 &= \sqrt{2}(11\sqrt{3}\cos\phi + \sqrt{3}\cos 3\phi \\
& & & \quad -12\sin\phi - 6\cos 2\phi \sin\phi) \\
C_3 &= (-2\cos^2\phi + \sin 2\phi)\cos\phi & D_3 &= -\cos\phi(21 + 9\cos 2\phi - 11\sqrt{3}\sin 2\phi) \\
C_4 &= (3 - \cos 2\phi - \sin 2\phi)\cos\phi & D_4 &= -\cos\phi(9 + 3\cos 2\phi - \sqrt{3}\sin 2\phi) \\
C_5 &= (1 + \cos 2\phi - \sin 2\phi)\sin\phi & D_5 &= (21 + 9\cos 2\phi - 11\sqrt{3}\sin 2\phi)\sin\phi \\
C_6 &= (3 - \cos 2\phi - \sin 2\phi)\sin\phi & D_6 &= (9 + 3\cos 2\phi - \sqrt{3}\sin 2\phi)\sin\phi.
\end{aligned}$$

References

[1] Gottstein G, Shvindlerman LS. Grain boundary migration in metals: thermodynamics, kinetics, applicationss. 2nd ed. Boca Raton (FL): CRC Press; 2010.
[2] Amelinckx S, Dekeyser W. Solid State Phys 1959;8:325.
[3] Lim AT, Srolovitz DJ, Haataja M. Acta Mater 2009;57:5013.
[4] Washburn J, Parker ER. J Metal 1952;4:1076.
[5] Gorkaya T, Molodov KD, Molodov DA, Gottstein G. Acta Mater 2011;59:5674.
[6] Janssens KGF, Olmsted D, Holm EA, Foiles SM, Plimpton SJ, Derlet PM. Nat Mater 2006;5:124.
[7] Olmsted DL, Holm EA, Foiles SM. Acta Mater 2009;57:3704.
[8] Li CH, Edwards EH, Washburn J, Parker ER. Acta Metall 1953;1:223.
[9] Bainbridge DW, Li CH, Edwards EH. Acta Metall 1954;2:322.
[10] Gottstein G, Molodov DA, Winning M, Shvindlerman LS. Interface Sci 2001;9:297.
[11] Winning M, Gottstein G, Shvindlerman LS. Acta Mater 2001;49:211.
[12] Winning M, Gottstein G, Shvindlerman LS. Acta Mater 2002;50:353.
[13] Badirujjaman S, Winning M. Metall Mater Trans A 2005;36:2905.
[14] Winning M, Rollett AD. Acta Mater 2005;53:2901.
[15] Cahn JW, Mishin Y, Suzuki A. Philos Mag 2006;86:3965.
[16] Cahn JW, Mishin Y, Suzuki A. Acta Mater 2006;54:4953.
[17] Badirujjaman S, Li XW, Winning M. Mater Sci Eng A 2007;448:242.
[18] Winning M. Philos Mag 2007;87:5017.
[19] Molodov DA, Ivanov VA, Gottstein G. Acta Mater 2007;55:1843.
[20] Gorkaya T, Molodov DA, Gottstein G. Acta Mater 2009;57:5396.
[21] Winning M, Rollett AD, Gottstein G, Srolovitz DJ, Lim A, Shvindlerman LS. Philos Mag 2010;90:3107.
[22] Molodov D, Gorkaya T, Gottstein G. J Mater Sci 2011;46:4318.
[23] Schönfelder B, Gottstein G, Shvindlerman LS. Acta Mater 2005;53:1597.
[24] Badirujjaman S, Winning M. Scripta Mater 2006;55:907.
[25] Schönfelder B, Gottstein G, Shvindlerman L. Metall Mater Trans A 2006;37:1757.
[26] Arsenlis A, Cai W, Tang M, Rhee M, Oppelstrup T, Hommes G, et al. Model Simul Mater Sci Eng 2007;15:553.
[27] Bulatov VV, Cai W. Computer simulations of dislocations. New York: Oxford University Press; 2006.
[28] Hirth JP, Lothe J. Theory of dislocations. 2nd ed. Malabar (FL): Krieger; 1992.
[29] Cai W, Bulatov V. Mater Sci Eng A 2004;387–389:277.
[30] Ohr SM, Beshers DN. Philos Mag 1963;8:1343.
[31] Cahn JW, Taylor JE. Acta Mater 2004;52:4887.
[32] Lücke K, Detert K. Acta Metall 1957;5:628.
[33] Cahn JW. Acta Metall 1962;10:789.
[34] Lücke K, Stüwe HP. Acta Metall 1971;19:1087.
[35] Mendelev MI, Srolovitz DJ, Weinan E. Philos Mag A 2001;81:2243.
[36] Mendelev MI, Srolovitz DJ. Model Simul Mater Sci Eng 2002;10:R79.